

Water Mass Variability in the Western North Pacific Detected in a 15-Year Eddy Resolving Ocean Reanalysis

YASUMASA MIYAZAWA^{1*}, RUOCHAO ZHANG¹, XINYU GUO^{1,2}, HITOSHI TAMURA¹, DAISUKE AMBE³, JOON-SOO LEE^{3†}, AKIRA OKUNO^{3††}, HIROSHI YOSHINARI^{3†††}, TAKASHI SETOU³ and KOSEI KOMATSU^{3,4}

¹Research Institute for Global Change, Japan Agency for Marine-Earth Science and Technology, Yokohama, Kanagawa 236-0001, Japan

²Center for Marine Environmental Studies, Ehime University, Matsuyama, Ehime 790-8577, Japan

³National Research Institute of Fisheries Science, Fisheries Research Agency, Yokohama, Kanagawa 236-8648, Japan

⁴Graduate School of Frontier Sciences, The University of Tokyo, Kashiwa, Chiba 277-8561, Japan

(Received 20 October 2008; in revised form 16 June 2009; accepted 26 June 2009)

This paper describes a reanalysis of the variability of water mass properties and currents in the western North Pacific using an ocean forecast system, Japan Coastal Ocean Predictability Experiment 2 (JCOPE2), to provide the basic description and information about the quality for data users. We have created the reanalysis data with high horizontal resolution of 1/12° to describe the oceanic variability associated with the Kuroshio-Kuroshio Extension, the Oyashio, and the mesoscale eddies from 1993 to 2007. The products made by an eddy-resolving ocean model combined with the three-dimensional variational data assimilation well reproduced the mean water mass property in the western North Pacific and the interannual variations of the Kuroshio-Kuroshio Extension and the Oyashio coastal branch. From the reanalysis data, we found that both the mean kinetic energy of the Kuroshio Extension axis at the first meandering crest and southward intrusion of the Oyashio coastal branch were closely related with the horizontal distribution of both the Oyashio Water and North Pacific Intermediate Water within the appropriate interannual time scale. The reanalysis data also indicated that the north-south migration of the Kuroshio Extension associated with its regime transitions affected the decadal modulation of the Subtropical Mode Water formation in the recirculation gyre of the Kuroshio Extension.

Keywords:

- Data assimilation,
- reanalysis,
- eddy-resolving model,
- western North Pacific,
- North Pacific Intermediate Water (NPIW),
- mode water,
- Kuroshio,
- Oyashio,
- Mixed Water Region.

1. Introduction

Combining ocean models and observation data, operational numerical ocean forecast has allowed us to predict variations of the western boundary currents and mesoscale eddies with a timescale of an order of 10 days (e.g., Ezer and Mellor, 1994; Kagimoto *et al.*, 2008). In such an operation, the model and observation data are

merged using a data assimilation technique (Daley, 1991) to prepare the initial state of the forecast. This merging procedure is usually called “analysis”. Since the analysis data (merged data) provides an optimum estimation of the oceanic condition based on both the model and observation, the analysis can be used to diagnose sparsely observed phenomena. To improve the forecast accuracy, however, the operational ocean forecast systems often require updates of parameters and numerical schemes included in the ocean models and data assimilation components. Thus the time sequences of the analyses sometimes show unrealistic jumps in state variables between before and after changes of the systems. To describe oceanic conditions during particular period in a consistent manner, it is quite useful to reconstruct the oceanic conditions without any change of the model and data assimilation schemes using almost all available observation data. This procedure is called “reanalysis”.

* Corresponding author. E-mail: miyazawa@jamstec.go.jp

† Present address: Ocean Climate Lab., Ocean Research Team, National Fisheries Research & Development Institute, Sirang-ri, Gijang-eup, Gijang-gun, Busan 619-902, Korea.

†† Present address: Japan Sea National Fisheries Research Institute, Fisheries Research Agency, Niigata 951-8121, Japan.

††† Present address: Hokkaido National Fisheries Research Institute, Fisheries Research Agency, Kushiro, Hokkaido 085-0802, Japan.

In the last several years, a number of ocean reanalyses over multi decades have become available and have been used for analyses of water mass variability. However, most of the available reanalyses are mapped on a horizontal coarse grid of approximately 1° (e.g., Carton and Santorelli, 2008). Our study is the first attempt to examine the interannual water mass variability in the western North Pacific using the ocean reanalysis data with a high horizontal resolution of $1/12^\circ$.

One of the important applications of reanalysis is statistical analysis to find the physical relationships between different physical variables, for example, between currents and water masses. To check the suitability of our data for this sort of analysis, we examined how the water mass variability associated with North Pacific Intermediate Water (NPIW) and Subtropical Mode Water (SMW) was statistically related to the ocean current variations using our reanalysis data.

The western North Pacific has a complicated ocean current system with significant water mass variability (e.g., Yasuda, 2003). The Kuroshio transports a large amount of warm and saline water to the south of Japan. The Kuroshio Extension formed by separation of the Kuroshio from the coast of Japan and the Oyashio which transports cold, fresh water creates the mixed water region east of Japan. The Kuroshio Extension is quite powerful; it makes stationary meanders and sheds warm and cold eddies through their separations from the meander crests and troughs. The Oyashio Water forms a front near the Japanese coast as a part of the subarctic front. Two branches of the Oyashio water, a coastal branch and an offshore branch, intrude southward from the Oyashio front and interact with the meander crests of the Kuroshio Extension and the warm eddies.

NPIW is characterized by a salinity minimum in intermediate layers of the subtropical region (e.g., Reid, 1965; Yoshinari *et al.*, 2004). Hasunuma (1978) suggested that the salinity minimum was not a sign of water mass but a boundary between the lower layer water originating from the subarctic region and the upper layer water originating from the subtropical region. Recent studies using high horizontal resolution temperature and salinity observations and high-resolution numerical modeling suggested that NPIW could be formed by isopycnal diffusion of the Oyashio and Kuroshio waters (Talley, 1993; Yasuda *et al.*, 1996; Ishizaki and Ishikawa, 2004) and by meridional overturning circulation with diapycnal and cross-gyre transports associated with water mass formation in the Okhotsk Sea (Yasuda, 1997; Tatebe and Yasuda, 2004). There are a few studies investigating interannual and decadal variations of NPIW. For example, Nakano *et al.* (2005) revealed that interannual variation of NPIW core size at 137°E was well correlated with that of the recirculation intensity associated with the intensity of the

subtropical gyre.

SMW is also one of the typical water masses in the northwestern subtropical region (Masuzawa, 1969). It is characterized by a pycnostad between the seasonal and main pycnoclines, and is formed by regional wintertime convective cooling (e.g., Suga and Hanawa, 1995b). Although the thickness of SMW in the western North Pacific is basically governed by the intensity of the winter monsoon, it is also influenced by the dynamic states of the Kuroshio and Kuroshio Extension (Suga and Hanawa, 1995a; Qiu and Chen, 2006; Qiu *et al.*, 2007).

As suggested by previous observational studies, the dynamic states of the Kuroshio, Kuroshio Extension, and Oyashio affect the water mass variability in the western North Pacific. In the mixed water region, because mesoscale eddy activities were very high, it has been difficult to investigate detailed relationships between the oceanic conditions and the variability of water mass properties owing to lack of long term hydrographic data with high horizontal resolution. By combining satellite altimetry data and dense observation by profiling floats, Qiu *et al.* (2007) recently showed that the mesoscale eddies actually weakened SMW's thickness in the recirculation region of the Kuroshio Extension within a period of less than 7 months.

In this paper we describe the 15-year eddy-resolving ocean reanalysis data from 1993 to 2007. Continuous operation of satellite altimetries after the launch of TOPEX/Poseidon in 1992 allowed us to reproduce the oceanic variability including the Kuroshio, its Extension paths and mesoscale eddies over the past 15 years (e.g., Uchida and Imawaki, 2003; Ambe *et al.*, 2004). We have reconstructed the oceanic states in the western North Pacific using a high-resolution ocean general circulation model together with the assimilation of both the satellite and in-situ data. Since the reanalysis data provide uniformly gridded oceanic states over particular period, it is useful for various kinds of studies. Some researchers have already used our data for their studies. The purpose of this study is to provide users with a basic description and information about the skills of our reanalysis data.

Previous version of the ocean forecast system (JCOPE1; Miyazawa *et al.*, 2004, 2005, 2008a; Kagimoto *et al.*, 2008) was used to analyze the Kuroshio path variation south of Japan. The water mass properties reproduced by JCOPE1 had significant biases in the western North Pacific despite data assimilation (Yoshinari *et al.*, 2008). We modified both the model and data assimilation schemes for better representation of the water mass properties in the western North Pacific, especially in the mixed water region. Our operational forecast system (<http://www.jamstec.go.jp/frcgc/jcope/>) has been updated to JCOPE2 from JCOPE1 in November 2006.

This paper is organized as follows. In Section 2, we

describe the configuration of the JCOPE2 ocean forecast system. In Section 3, we present climatological mean states of the 15-year data. In Section 4, we describe skills of the 15-year data for variability of the Kuroshio, Kuroshio Extension, and Oyashio coastal branch. Then we discuss the relationships between the interannual variation of the oceanic conditions and that of both NPIW and SMW as found in the 15-year data. Section 5 contains a final summary and discussion.

2. The JCOPE2 Ocean Forecast System

2.1 Ocean model

The ocean model in the JCOPE2 system is based on the Princeton Ocean Model with a generalized coordinate of sigma (POMgcs; Mellor *et al.*, 2002). A high-resolution regional model with a spatial grid of $1/12^\circ$ and 46 vertical levels was embedded in a low-resolution model with a spatial grid of approximately $1/4^\circ$ and 21 sigma levels, covering the almost entire Pacific region (30°S – 62°N , 100°E – 90°W). The bottom topography of the low-resolution model was created from the $1/12^\circ$ global height data, GETECH DTM5. The lateral boundary conditions of the low-resolution model are the monthly climatological temperature and salinity (Conkright *et al.*, 2002) with zero velocity.

The inner high-resolution model domain covers the western North Pacific (10.5° – 62°N , 108° – 180°E); and its lateral boundary conditions are determined from the basin-wide model using a one-way nesting method with the flow relaxation scheme (Oey and Chen, 1992; Guo *et al.*, 2003). The bottom topography of the high-resolution model was also created from the $1/12^\circ$ data, DTM5. In addition, the $1/108^\circ$ data, JTOPO30, was embedded in the coastal sea around Japan and the $1/12^\circ$ bottom topography data used by Uehara *et al.* (2002) was embedded in the East China Sea.

Because the western North Pacific has a wide range of variability in both the bottom topography and water mass properties, some errors in the baroclinic pressure gradient generated in the sigma coordinate systems with a steep bottom slope may contaminate the calculation (Mellor *et al.*, 1994). Thus, the bottom topography in both the low- and high-resolution models has been smoothed to reduce the pressure gradient error (Mellor *et al.*, 1994). The maximum bottom slope between two adjacent grid points was constrained by the inequality, $|H1 - H2|/|H1 + H2| \leq 0.15$. In addition, we have modified the POMgcs to reduce the errors by replacing the second order scheme of baroclinic pressure gradient with the fourth order (McCalpin, 1994).

To exclude small scale noises in temperature and salinity distributions, we replaced the central advection and harmonic diffusion schemes for temperature and sa-

linity with the flux-corrected transport (Boris and Book, 1973) and bi-harmonic schemes (Griffies and Hallberg, 2000), respectively. The horizontal viscosity was calculated by the Smagorinsky-type formulation with a coefficient of 0.2. The horizontal diffusivity coefficient was assumed to be one-half of the viscosity coefficient.

The model was driven by wind stresses, and heat and salt fluxes. The wind stress and heat flux fields were calculated from the 6-hourly National Centers for Environmental Prediction/National Center for Atmospheric Research (NCEP/NCAR) reanalysis data (Kalnay *et al.*, 1996), using bulk formulae (Kagimoto *et al.*, 2008). Instead of the observed sea surface temperature with horizontal coarse resolution (2°) included in the NCEP/NCAR data, the high-resolution model used its output of sea surface temperatures for the calculation of the bulk formulae. This improved the low (high) surface temperature bias in the marginal seas in winter (summer). Salinity at the ocean surface is restored to the monthly mean climatology data (Conkright *et al.*, 2002) with a time scale of 30 days. In both the Okhotsk and Bering Seas, temperature and salinity are relaxed to the monthly climatology (Conkright *et al.*, 2002) with a restoring time scale of 30 days to improve water mass property in the Mixed Water Region (Mitsudera *et al.*, 2004).

The low-resolution model is spun-up for 15 years by the monthly mean surface forcing from an initial condition of no motion with the annual-mean temperature and salinity fields created from the climatology (Conkright *et al.*, 2002). The high-resolution model is also run from the same initial condition. The lateral boundary condition of the 5-year spin-up run of the high-resolution model is calculated using the spin-up results of the low-resolution model over the last 5 years. Then both the low- and high-resolution models are driven by the 6-hourly surface forcing during the period from October 1992 to January 2008.

2.2 Data assimilation

The following observation data were assimilated into the model: along-track sea surface height anomaly (SSHA) obtained from the TOPEX/Poseidon and ERS-1, 2 satellites during the period December 1992 to January 2002 and from the Jason-1 and Geosat Follow-On during the period January 2002 to January 2008; sea surface temperature (SST) obtained from the Advanced Very High Resolution Radiometer/Multi-Channel Sea Surface Temperature (AVHRR/MCSST) products; and vertical profiles of temperature and salinity obtained from the data archive of the Global Temperature-Salinity Profile Program (GTSP; see <http://www.nodc.noaa.gov/GTSPP/index.html>). We used the delayed-mode archive of GTSP (“Best Copy Data Sets”), which were assembled to provide the most complete data sets without duplication.

Notice that the GTSPP archive includes no salinity profiles from 1995 to 1999 in the western North Pacific, which slightly affected the accuracy of the reanalysis data (see Section 3).

The data assimilation procedure in our system comprises two steps: the creation of temperature-salinity analysis data on a three-dimensional uniform grid by the variational assimilation method (Fujii and Kamachi, 2003), and incremental analysis update (IAU) (Bloom *et al.*, 1996) of the analysis data for smooth initialization.

The variational assimilation method minimizes a cost function that represents the sum of the square distances between the analysis and the observations. The grid of the analysis temperature and salinity has horizontal resolution of $1/4^\circ$ and 24 vertical levels on the z -coordinate from a depth of 0 m to 1500 m. The cost function J is written in the form of a function of the analysis temperature and salinity (X),

$$\begin{aligned}
J(X) = & (X - X^f)^t B^{-1} (X - X^f) \\
& + (y_T^o - H_T X)^t R_T^{-1} (y_T^o - H_T X) \\
& + (y_S^o - H_S X)^t R_S^{-1} (y_S^o - H_S X) \\
& + (y_{SSHA}^o - H_{SSHA}(X))^t R_{SSHA}^{-1} (y_{SSHA}^o - H_{SSHA}(X)) \\
& + (y_{SST}^o - H_{SST} X)^t R_{SST}^{-1} (y_{SST}^o - H_{SST} X), \quad (1)
\end{aligned}$$

where B is the background error covariance matrix for the first guess; y^o is a column vector whose elements are the observed variables; H denotes an operator for a projection from the model variables to the observed variables. H_T , H_S and H_{SST} are bilinear interpolation operators. H_{SSHA} is a nonlinear operator for calculation of the sea surface dynamic height; R denotes an observation error covariance matrix. At the time of the analysis, by minimizing the cost function (1) with the use of a conjugate gradient method, we obtained the analysis temperature and salinity. We created the analysis with an interval of 7 days. The time windows of observed SSHA, SST, and vertical profiles of temperature and salinity used in the cost function (1) are 10, 10, and 20 days, respectively.

By using temperature and salinity coupling EOF modes (E_{Ti} , E_{Si}), the analysis temperature (T) and salinity (S) are represented as follows:

$$X = (T, S) = (T^f, S^f) + \sum_{i=1}^M \alpha_i \lambda_i (D_{Tz} E_{Ti}, D_{Sz} E_{Si}), \quad (2)$$

where $X^f = (T^f, S^f)$ are first guess values; α_i are ampli-

tudes of the EOF mode; $D_{T(S)z}$ are standard deviations of temperature (salinity) variations at z levels calculated from the historical data archives; and λ_i are the singular values of the EOF mode. The control variables of the analysis temperature and salinity for the cost function (1) are amplitudes of the EOF modes, α_i . We calculated the EOF modes from the historical data archives of temperature and salinity profiles (World Ocean Database 2001) and Marine Information Research Center Ocean Data Set 2001) in six regions: subarctic region (39.5° – 55° N, 140° – 180° E); mixed water region (37° – 45° N, 140° – 180° E); Kuroshio–Kuroshio Extension region (22° – 33° N, 120° – 180° E); subtropical region (12° – 27.5° N, 120° – 180° E); the southern part of the Japan Sea (35° – 39° N); and the northern part of the Japan Sea (41° – 53° N). Because the first twelve modes can represent over 95% of the observed variability in all regions, we used the first twelve EOF modes for calculation of the analysis, i.e., $M = 12$ in (2).

Although the three-dimensional variational assimilation method using the temperature-salinity coupling EOF modes has already been used in the other type of the operational ocean forecasting model (Usui *et al.*, 2006), it was quite important to customize the data assimilation method for an individual ocean model by investigating sensitivities of the parameters. We found that relatively sensitive parameters for the estimation of the analysis temperature and salinity using the minimization of the cost function (1) were the EOF modes (E_{Ti} , E_{Si}), error covariance matrices B and R , first guess X^f , and the mean sea surface dynamic height (SSDH) field that is necessary for calculation of the model SSHA.

We assumed that the components of the background error covariance matrix B have horizontal correlation that is supposed to be a Gaussian function:

$$\exp(-x^2 / S_x^2 - y^2 / S_y^2), \quad (3)$$

where x and y are distances between the grid points along eastward and northward directions, respectively; S_x and S_y are horizontal scales that were assumed to be constants in the regions except for the Kuroshio-Kuroshio Extension region (see Appendix) and determined according to the estimates obtained by the statistical analysis of satellite altimeters (Kuragano and Kamachi, 1999).

The observation covariance R was supposed to be a diagonal matrix; the observation data have no correlation with each other. We assumed that the observation error of the satellite SST was 1.0° C and that of SSHA was 0.05 m except for the Kuroshio-Kuroshio Extension region (see Appendix). The observation error of in-situ temperature and salinity was specified as follows:

$$T_{err}^o = (1 - \sigma) S_{Tz}, \quad S_{err}^o = (1 - \sigma) S_{Sz} \quad (\sigma = 0.7 - 0.9). \quad (4)$$

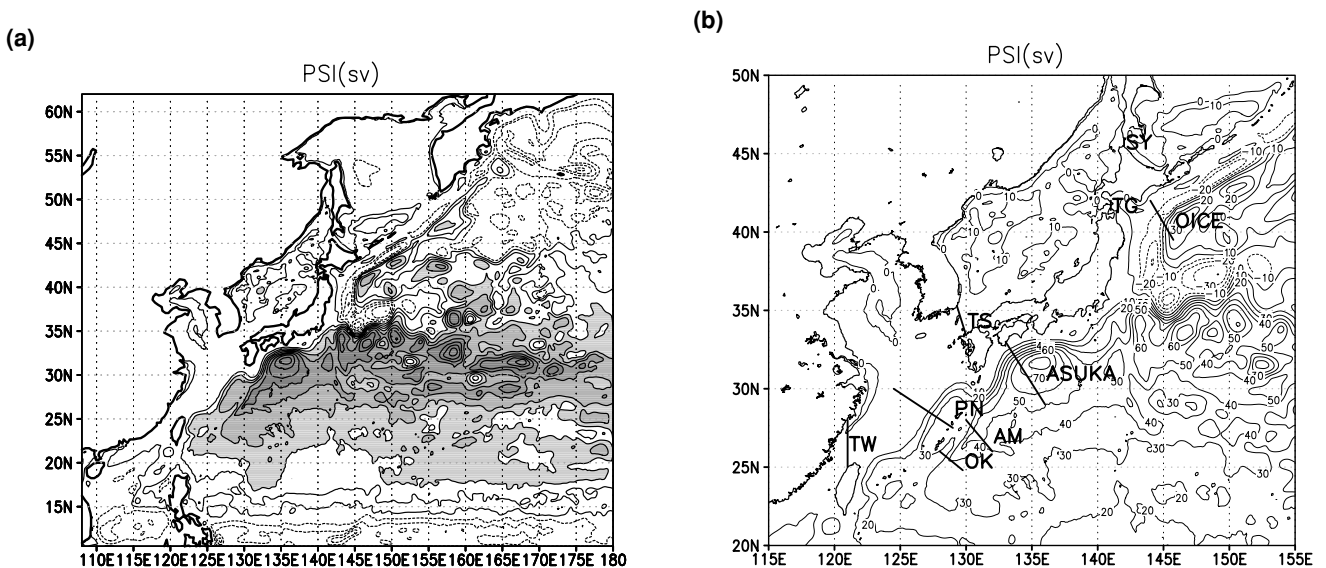


Fig. 1. (a) Volume transport stream function of mean flow calculated from the reanalysis data within 1993 to 2007. Contour interval is 10 Sv. Regions of the stream function upper than 20 Sv are shaded. (b) As in (a) except for the magnified view showing the Japanese coastal ocean. Lines indicate sections along which the mean volume transports were calculated (Table 1).

The prescribed error of first guess temperature and salinity was related with the observation error.

$$T_{err}^f = \sigma T_z, \quad S_{err}^f = \sigma S_z \quad (\sigma = 0.7 - 0.9). \quad (5)$$

The parameter σ provides the relative weight of the first guess temperature and salinity compared to the observation.

We used both the climatology data X_{clim} and model variables X_{model} for the first guess:

$$X^f = W_{clim} X_{clim} + (1 - W_{clim}) X_{model}$$

$$W_{clim} = \min(\max(W, 0), 1), \quad W = \frac{|Grad_h| - |Grad_h^{max}|}{|Grad_h^{min}| - |Grad_h^{max}|}, \quad (6)$$

where $Grad_h$ is the horizontal gradient of temperature at 200 m depth; $||$ indicates the two-dimensional vector norm. Scheme (6) increases the weight of the model (climatology) for the first guess value at the grid point where the horizontal temperature gradient is large (small). Use of scheme (6) significantly reduced biases involved in the water mass property represented by the assimilation product.

The mean SSDH is necessary to calculate the model SSHA because not SSDH but SSHA of the satellite altimeter is available from the satellite altimeters. We calculated the mean SSDH from the annual mean climatol-

ogy (Conkright *et al.*, 2002) and modified the obtained mean SSDH in the Kuroshio region with that from a previous version of our ocean forecast system (JCOPE1; Kagimoto *et al.*, 2008; Miyazawa *et al.*, 2008a). This is because that the Kuroshio path southeast of the Kii Peninsula appearing in the SSDH calculated from the annual mean climatology was similar to the large meander path, but the observed mean Kuroshio path during the assimilation period from 1993 to 2007 was the non-large meander path. Thus only for the Kuroshio region, we used the mean SSDH from the JCOPE1 product over the period from November 2002 to October 2006 during which the mean Kuroshio path was the non-large meander path (Miyazawa *et al.*, 2008a).

Using the analysis temperature and salinity, we conducted the IAU procedure for data from December 1992 to January 2008 and stored the daily mean data, referred to as the reanalysis data. The reanalysis data from January 1993 to December 2007 were used for the present analysis.

3. Mean State and Water Mass Properties Reproduced by the Reanalysis Data from 1993 to 2007

Figure 1(a) shows the volume transport stream function calculated from the mean velocity field of the 15-year reanalysis data. The subtropical gyre, which consists of the North Equatorial Current, Kuroshio, and Kuroshio Extension, is well represented. The Ryukyu Current east of the Kuroshio main stream in the East China Sea (Zhu *et al.*, 2003) and the Kuroshio recirculation south

Table 1. Comparison of volume transports (Sv) between the reanalysis and observation data. The transports of the reanalysis data were calculated from surface to bottom along the several sections across the main currents in the Japanese coastal oceans. The names of the sections (see Fig. 1(b)) are shown in the parentheses.

| Currents | Reanalysis | Observations |
|-------------------------------------|------------|--------------------------------------|
| Taiwan Strait Current (TW) | 1.4 | 1.8 (Wang <i>et al.</i> , 2003) |
| Kuroshio in the East China Sea (PN) | 32.7 | 25.4 (Hinada, 1996) |
| Ryukyu Current (OK) | 6.9 | 6.1 (Zhu <i>et al.</i> , 2003) |
| Ryukyu Current (AM) | 6.0 | 16 (Ichikawa <i>et al.</i> , 2004) |
| Kuroshio south of Japan (ASUKA) | 49.0 | 42 (Imawaki <i>et al.</i> , 2001) |
| Tsushima Warm Current (TS) | 2.5 | 2.64 (Takikawa <i>et al.</i> , 2005) |
| Tsugaru Warm Current (TG) | 2.1 | 1.4 (Shikama, 1994) |
| Soya Warm Current (SY) | 0.4 | 0.7 (Ebuchi <i>et al.</i> , 2006) |
| Oyashio (OICE, southwestward) | 41.0 | 31 (Uehara <i>et al.</i> , 2004) |

of the Shikoku Island (Imawaki *et al.*, 2001) can also be identified. The mean Kuroshio path southeast of the Kii Peninsula during the reanalysis period from 1993 to 2007 is the non-large meander path (Miyazawa *et al.*, 2008a). The reanalysis produces a strong flow of the Kuroshio Extension with the two crests at $143^{\circ}E$ and $148^{\circ}E$. The intensity of the Kuroshio Extension weakens east of $155^{\circ}E$, indicating its bifurcation around the Shatsky Rise. These features of the Kuroshio Extension are consistent with observation (Mizuno and White, 1983). The East Kamchatka current originates from the Bering Sea and flows southwestward along the continental slope. The cyclonic circulation accompanied with the Oyashio coastal intrusion along the Honshu Island intensifies the Kuroshio Extension. The return flow of the Oyashio together with the strong recirculation flow forms the coastal and offshore branches of the Oyashio. We compared mean volume transports along some sections (Fig. 1(b)) across the main currents with the observed data (Table 1). The reanalysis transports were of the same order as those reported by previous studies.

To check the accuracy of the reanalysis data for the mean water mass properties of the western North Pacific, we compared the reproduced temperature and salinity profiles with the observed profiles in detail. Since the reanalysis combines the information of remote and in-situ observations by assimilating SSHa, SST, and in-situ profiles obtained from the GTSP archive, we examined the fit of the reanalysis data for the GTSP profiles to check whether the assimilation worked well or not. We compared temperature-salinity diagrams of the reanalysis data with diagrams of in-situ observed profiles averaged over the period from 1993 to 2007 (Fig. 2). The diagrams of the reanalysis data correspond fairly closely with the observations in the subarctic, mixed water, subtropical regions, respectively (see Fig. 3 for locations of the regions). The results suggest that the system has assimilated

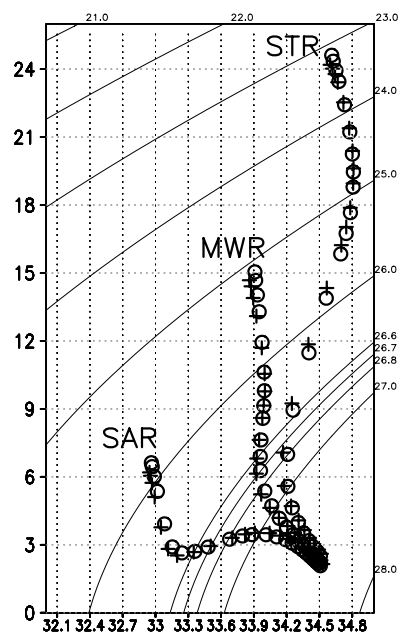


Fig. 2. Temperature-salinity diagram of mean profiles from the reanalysis (open circles) and the in-situ observation data included in the GTSP archive (crosses). Left, middle, and right profiles were means of the data in 45° – $60^{\circ}N$, 155° – $175^{\circ}E$ (Subarctic Region; SAR), 35° – $45^{\circ}N$, 142° – $172^{\circ}E$ (Mixed Water Region; MWR), and 20° – $35^{\circ}N$, 130° – $150^{\circ}E$ (Subtropical Region; STR), respectively. Contour lines denote iso- σ_{θ} contours.

the in-situ observation profiles with only small biases.

To examine spatial differences in the reproduction skills, we plotted Root Mean Square Error (RMSE), mean error (bias), and correlation between the reanalysis and observed profiles from the surface to a maximum depth of 1500 m (Fig. 3). The mixed water region shows RMSE

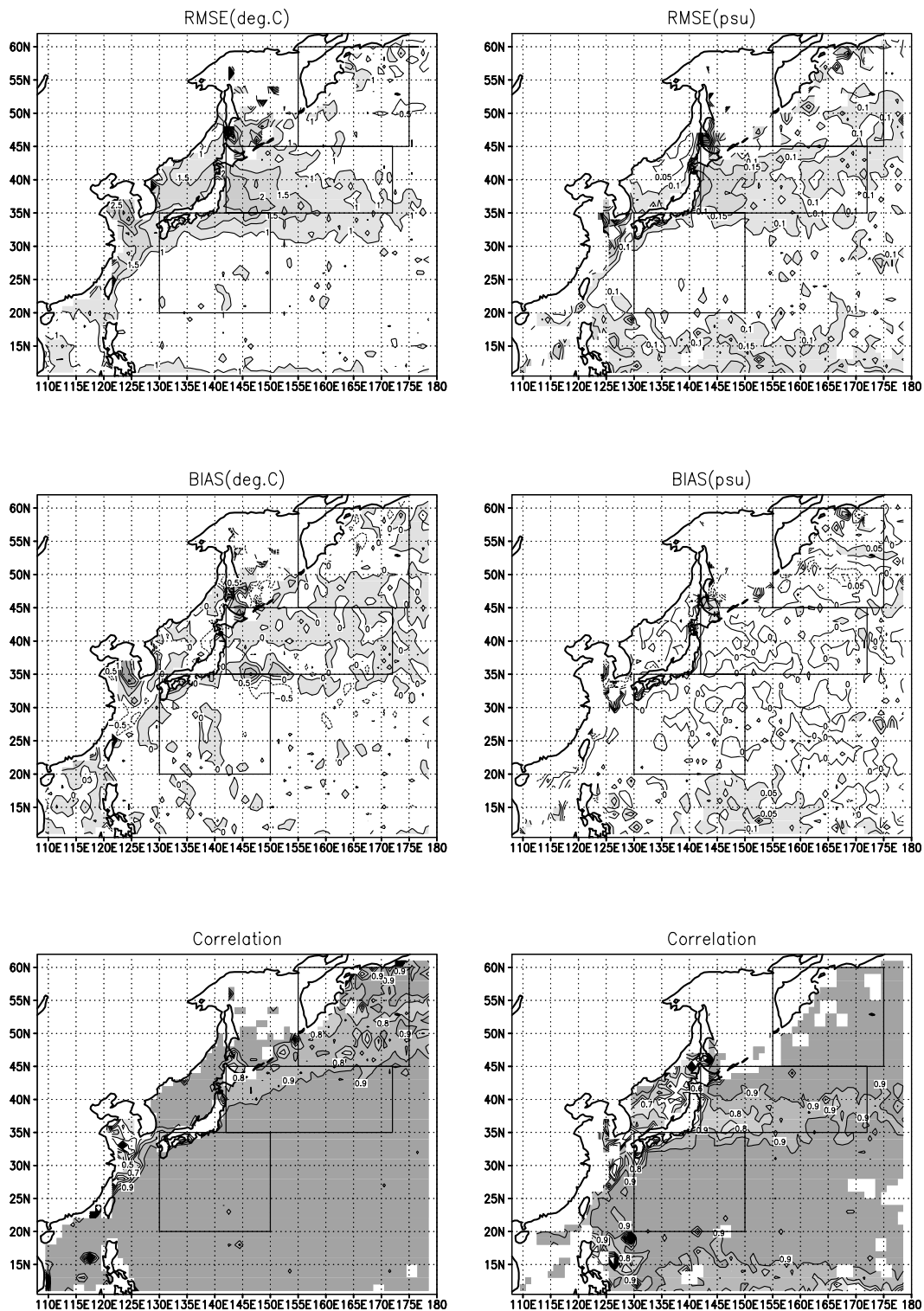


Fig. 3. Root Mean Square Error (RMSE; upper panels), mean error (bias; middle panels), and correlation of the temperature (left panels) and salinity (right panels) profiles of the reanalysis data by those of the in-situ observation obtained from the GTSPP archive. Rectangles in the panels indicate the subarctic, mixed water, and subtropical regions used for the calculations of metrics shown in Figs. 2 and 4.

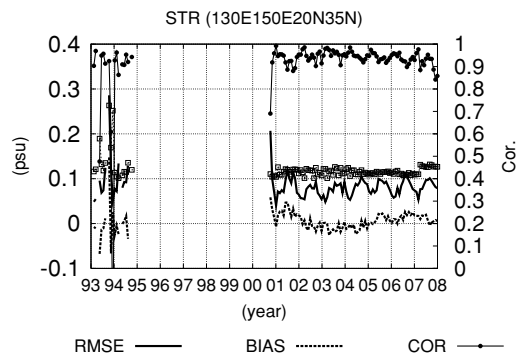
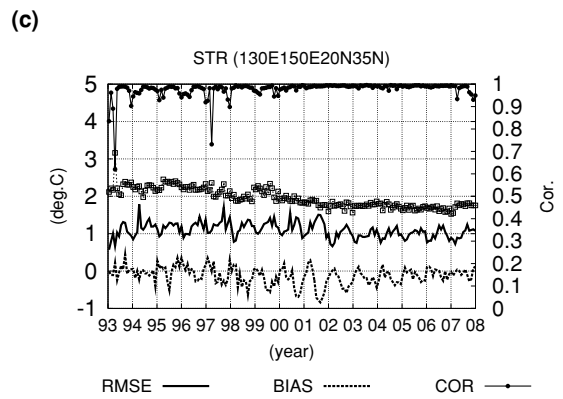
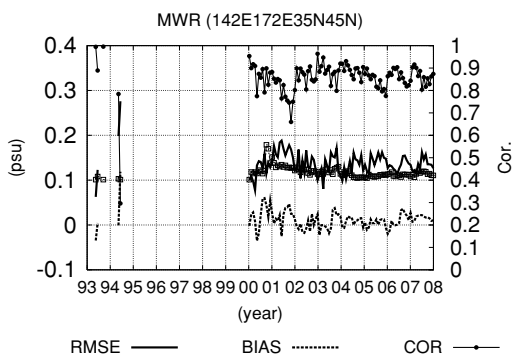
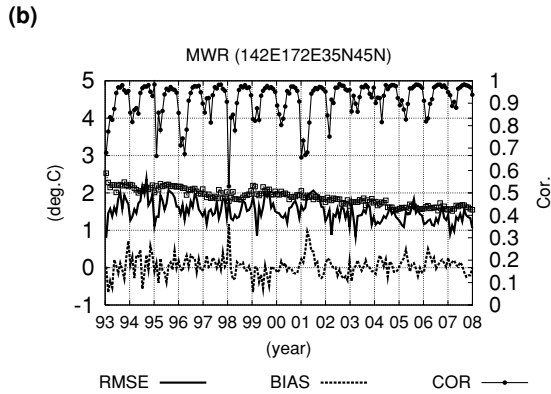
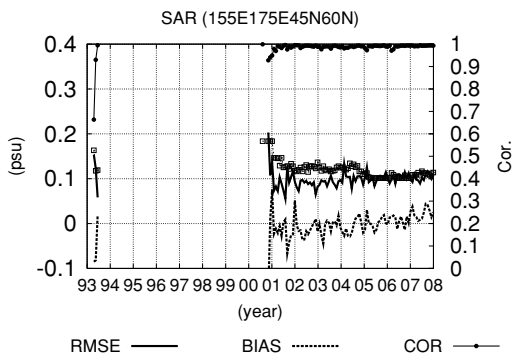
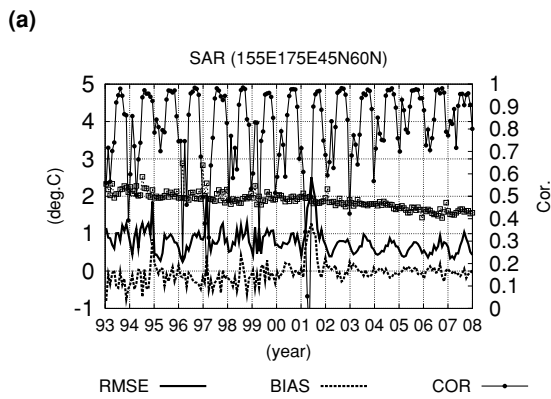


Fig. 4. Time sequences of Root Mean Square Error (RMSE; thick solid curves), mean error (bias; dashed curves) of the temperature (upper panels) and salinity (lower panels) profiles of the reanalysis data for those of the GTSP data. Correlation and minimum correlation values required for statistical significance at the 95% confidence level are also indicated by thin solid curves with closed circles and dotted curves with open squares, respectively. (a), (b), and (c) show averaged values in 45° – 60° N, 155° – 175° E (the subarctic region), 35° – 45° N, 142° – 172° E (the mixed water region), and 20° – 35° N, 30° – 150° E (the subtropical region), respectively.

higher than 2° C and 0.15 psu east of Japan (upper panels of Fig. 3) because of the large water mass variability there. Since RMSE is smaller than the standard deviation of the observed profiles (not shown), the model has passable accuracy for the assimilation of the in-situ profiles there. The Japan Sea shows RMSE higher than 1.5° C and 0.1 psu but it is also smaller than the observed standard deviations. In the shelf region of the East China Sea, RMSE is comparably large compared to the observed standard deviation owing to there being no assimilation of in-situ profiles there. In the Pacific, regions of positive temperature bias higher than 0.5° C are shown around 35° N and 145° – 155° E (middle panels of Fig. 3). This is because the mean Kuroshio Extension path is more north than the one observed there (see Subsection 4.1). The shelf region

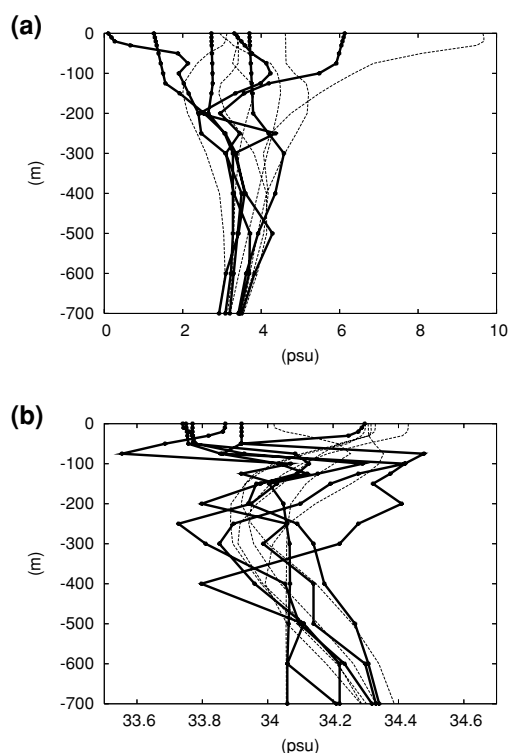


Fig. 5. (a) Temperature profiles of the observation (solid curves with closed circles) and reanalysis data (dashed curves) sampled from 40°–62°N and 140°–180°E in February 2001. The profiles that have correlation values lower than 0.3 are selected. (b) Same as in (a) except for salinity profiles sampled from 35°–45°N and 140°–180°E in November 2001.

of the East China Sea shows positive temperature and low salinity biases. Correlation coefficients for temperature and salinity are relatively low in this region (lower panels of Fig. 3). In the subarctic regions, correlation is low for temperature but high for salinity. The lower right panel of Fig. 3 indicates slightly low correlation for salinity in the mixed water region, shelf of the East China Sea, Japan Sea, and near the southern boundary for salinity. In summary, the reanalysis data is reasonably accurate for water mass representation in the western North Pacific.

Figure 4 plots time sequences of RMSE, bias, and correlations of the reanalysis data averaged in the subarctic (Fig. 4(a)), mixed water (Fig. 4(b)), and subtropical regions (Fig. 4(c)). Since no salinity profile is archived in GTSP from 1995 to 1999 for all the three regions, no precise information for salinity is shown during this period. The effectiveness for the subtropical region is stable throughout the reanalysis period except for salinity in 1993 and 2001.

In the subarctic regions, the correlation for temperature varies with the seasonal time scale; the fit is worse

from winter to spring than from summer to autumn. It was found that the reanalysis data sometimes failed to represent the surface cooling associated with the mesothermal structure (intermediate temperature maximum; Uda, 1963) in the subarctic and mixed water regions. Figure 5(a) is an example indicating that surface temperature of the reanalysis data in the subarctic regions had warmer bias in winter.

In the mixed water region, the correlation for salinity shows a temporal variation (lower panel of Fig. 4(b)). Also, the correlation value averaged over the reanalysis period was relatively low in this region compared to that in the other regions (lower right panel of Fig. 3). Figure 5(b) depicts comparison of some salinity profiles in November 2001, which showed the lowest correlation value of monthly average (0.66) during the reanalysis period (lower panel of Fig. 4(b)). The observed profiles had more complicated features than the reanalysis profiles. In particular, the reanalysis data did not reproduce low surface salinity because the surface salinity in the reanalysis data was basically relaxed to the monthly climatology through the surface boundary condition and the assimilation at this time did not effectively correct the temporal and spatial variations in surface salinity. The mixed water region is included in the storm track region of the western North Pacific involving the large variability in precipitation. Then enough amounts of the salinity observation and/or more reliable surface boundary condition of salinity are required to reproduce well the variations of surface salinity in this region.

Note that the fluctuation of the correlation for both temperature and salinity was moderated from 2002 to 2007 due to the increase of the number of assimilated in-situ profiles after the launch of the Argo floats deployments (Feder, 2000).

4. Water Mass Variability Detected in the Reanalysis Data

The Kuroshio-Kuroshio Extension, Oyashio southward intrusion, and mesoscale eddies play important roles in water mass variability of the western North Pacific (e.g., Yasuda, 2003). We investigated the skill of the reanalysis data for the path variations of the Kuroshio-Kuroshio Extension, the eddy kinetic energy in the mixed water region, and the southern end latitude of the Oyashio coastal branch. Then using the reanalysis data, we examined relations between the variations of the oceanic conditions described above and the water mass variability of NPIW and SMW.

4.1 Variability of the Kuroshio Extension

It is well known that the Kuroshio south of Japan has two stable paths: a large meander path and a non-large meander path (Yoshida, 1964). During the reanalysis

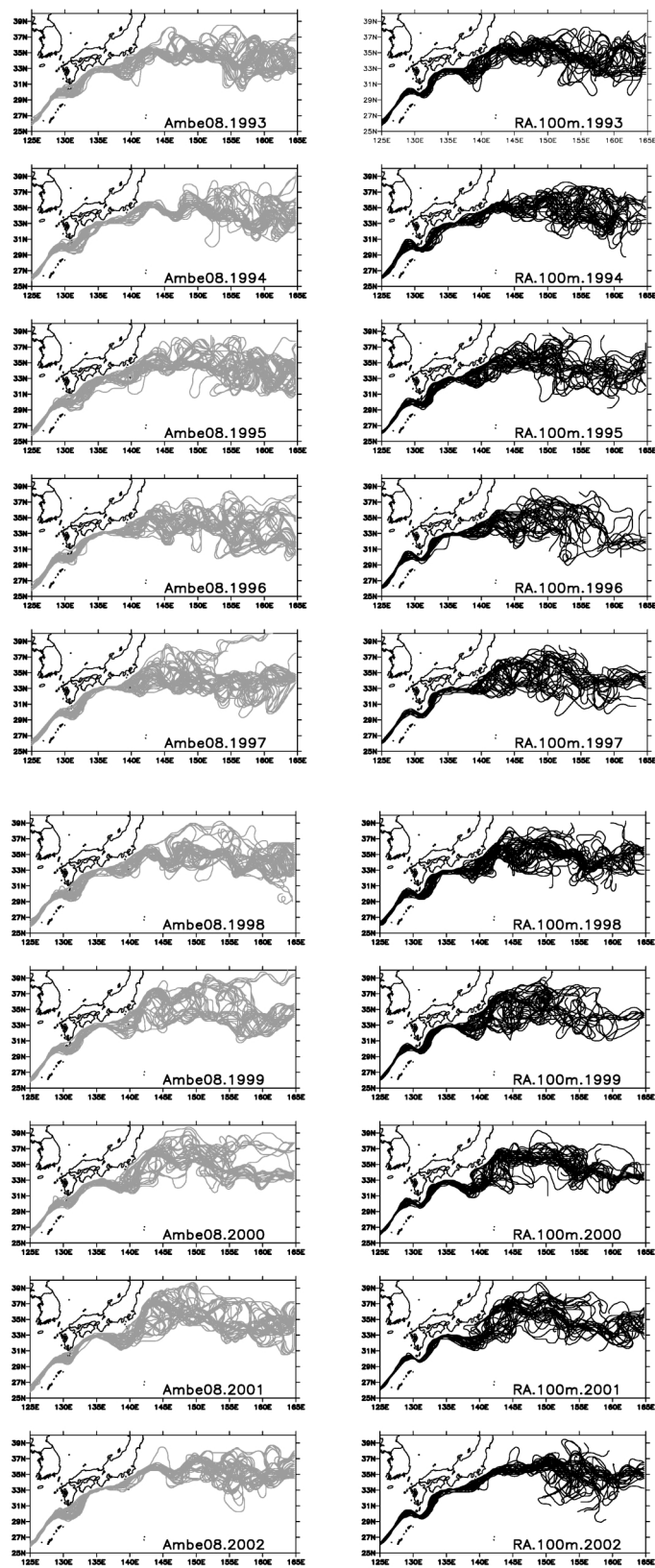


Fig. 6. The Kuroshio-Kuroshio Extension paths estimated at weekly interval in each year from 1993 to 2007. Left: estimated from the surface layer velocities data calculated using drifting buoy and satellite altimetries (Ambe08). Right: estimated from the velocities of the reanalysis data at 100 m depth.

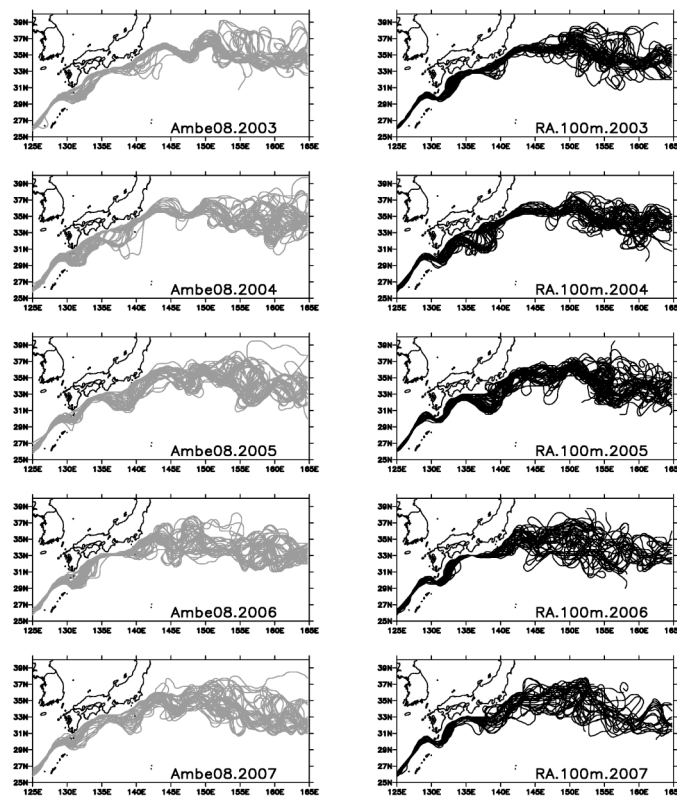


Fig. 6. (continued).

period from 1993 to 2007, the Kuroshio almost always took the non-large meander path except during the 1-year period of the large meander, August 2004 to August 2005 (Miyazawa *et al.*, 2008a). Using the satellite altimetry data, recent observational studies (e.g., Qiu *et al.*, 2007) have discovered that the Kuroshio Extension has two dynamic regimes: the stable and unstable states. Qiu *et al.* (2007) showed that the eddy kinetic energy associated with the Kuroshio Extension path variation was low from October 1992 to mid-1996 and from the beginning of 2002 to the end of 2004, and high from mid-1996 to the end of 2001 and from the beginning of 2005 to mid-2006.

To examine the skill of the reanalysis data for the path variations of the Kuroshio and Kuroshio Extension, we compared path latitudes of the Kuroshio-Kuroshio Extension in the reanalysis data with the observed latitudes estimated from the gridded surface geostrophic current velocity data with a horizontal resolution of $1/4^\circ$ (Ambe, D., K. Komatsu, M. Shimizu, and A. Okuno, 2009, unpublished manuscript; hereafter Ambe08). Ambe08 is an updated and extended version of the velocity data made by combining the historical data archive of drifting buoys and satellite SSHA data (Uchida and Imawaki, 2003; hereafter UI2003). UI2003 is quite useful to effectively

estimate the Kuroshio path (Ambe *et al.*, 2004).

We estimated the position of the Kuroshio-Kuroshio Extension path by tracking the grid points of maximum kinetic energy for velocities at 100 m depth in the reanalysis data and those for the velocities in Ambe08. The reason we chose 100 m depth is to avoid the contamination of ageostrophic components. Figure 6 compares the reanalysis and observed weekly Kuroshio-Kuroshio Extension path from 1993 to 2007. The reanalysis data likely reproduces both the large (August 2004 to July 2005) and non-large meander (January 1993–July 2004 and August 2005–December 2007) states of the Kuroshio south of Japan, and both the unstable (1996–2001 and 2005–2007) and stable (1993–1995 and 2002–2004) states of the Kuroshio Extension.

The Kuroshio path variation south of Japan is relatively stable compared with that of the Kuroshio Extension. As shown in Fig. 7(a), west of 140°E , RMSE of the path latitude of the reanalysis data for that of Ambe08 is within approximately 50 km but increases to 150 km east of 140°E . The absolute value of the mean error (bias) of the path position indicated by a dashed curve is within 30 km except for 50 km between 145° and 152°E . We also compared the mean kinetic energy measured along the Kuroshio-Kuroshio Extension path for the reanalysis data

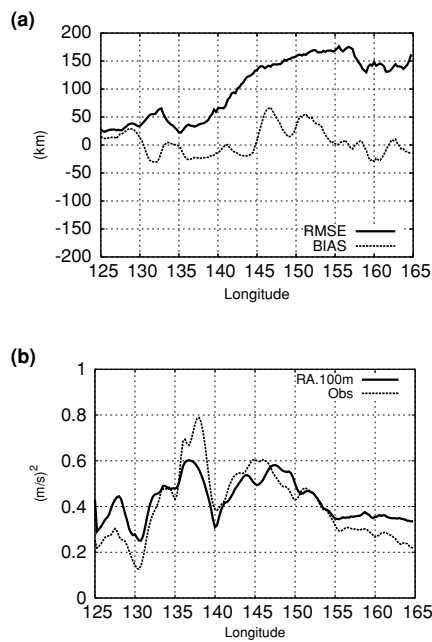


Fig. 7. (a) Root Mean Square Error (RMSE; solid curve) and mean error (bias; dashed curve) of the latitudes of the reanalysis Kuroshio-Kuroshio Extension paths (right panels of Fig. 6) by the Ambe08 paths (left panels of Fig. 6). (b) Mean kinetic energy distributions along the Kuroshio-Kuroshio Extension paths calculated from the reanalysis (solid curve) and Ambe08 data (dashed curve).

and Ambe08 (Fig. 7(b)). The reanalysis data basically reproduced distribution of the mean kinetic energy on the Kuroshio-Kuroshio Extension path.

In the previous version of the JCOPE model (JCOPE1), the Kuroshio Extension path exhibited a strong southward bias, with a maximum deviation of 100 km. The mean kinetic energy of the Kuroshio Extension in JCOPE1 was approximately half the magnitude observed (Miyazawa, 2007). The most significant difference between JCOPE1 (Miyazawa *et al.*, 2008a) and JCOPE2 systems is the data assimilation component; JCOPE1 (JCOPE2) adopted the multivariate optimum interpolation (the three-dimensional variational assimilation). The variational assimilation used the temperature and salinity coupling EOF modes obtained from the in-situ observation data to describe vertical relationships between the surface (e.g., SSHA or SST) and the subsurface (e.g., temperature and salinity) variables, which were quite important for the representation of water mass properties. Regression coefficients obtained from the model simulation, which were used in the multivariate optimum interpolation of JCOPE1, caused biases of the water mass properties and the Kuroshio Extension path (Yoshinari *et al.*, 2008).

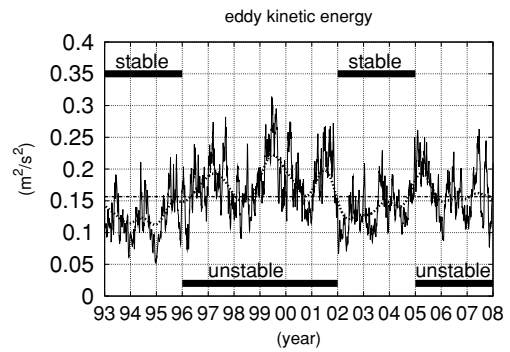


Fig. 8. Time sequences of surface eddy kinetic energy of the reanalysis data averaged in 32°–38°N and 141°–153°E. The eddy kinetic energy was calculated from SSHA using geostrophic flow approximation. Solid (dashed) curve indicates daily mean values (band-pass-filtered values within periods from 1 year to 10 years). Thick lines denote stable and unstable years of the Kuroshio Extension. Dash dotted line indicates the temporal average magnitude, 0.157 m²s⁻².

Table 2. Standard deviations of the indices associated with the dynamical regimes of the Kuroshio Extension indicating (a) the northern latitude of the first meandering crest (in degrees; NLFCKE) and (b) its mean kinetic energy (in m²s⁻¹; MKE). Standard deviations of the daily mean data were calculated for the band-pass-filtered values. Numbers in the parenthese denote the mean values.

| | Ambe08 | Reanalysis data |
|----------------------|-------------|-----------------|
| (a) NLFCKE | | |
| Stable (1993–1997) | 0.80 (35.8) | 0.58 (36.0) |
| Unstable (1996–2001) | 0.84 (36.5) | 0.92 (36.4) |
| Stable (2002–2004) | 0.37 (36.0) | 0.37 (36.0) |
| Unstable (2005–2007) | 0.70 (35.9) | 0.61 (36.0) |
| (b) MKE | | |
| Stable (1993–1997) | 0.09 (0.52) | 0.11 (0.43) |
| Unstable (1996–2001) | 0.10 (0.47) | 0.14 (0.43) |
| Stable (2002–2004) | 0.09 (0.66) | 0.11 (0.65) |
| Unstable (2005–2007) | 0.10 (0.55) | 0.14 (0.50) |

The eddy kinetic energy calculated from the reanalysis SSHA (Fig. 8) shows the transitions between stable and unstable states similar to those reported by the previous studies (e.g., see figure 4b in Qiu and Chen, 2006). From Fig. 8, we can define the stable (unstable) years as being 1993 to 1995 (1996 to 2001) and 2002 to 2004 (2005 to 2007) comparing the eddy kinetic energy with its average magnitude, 0.157 m²s⁻². We calculated the following indices from both the reanalysis data and Ambe08: the northernmost latitude and mean kinetic en-

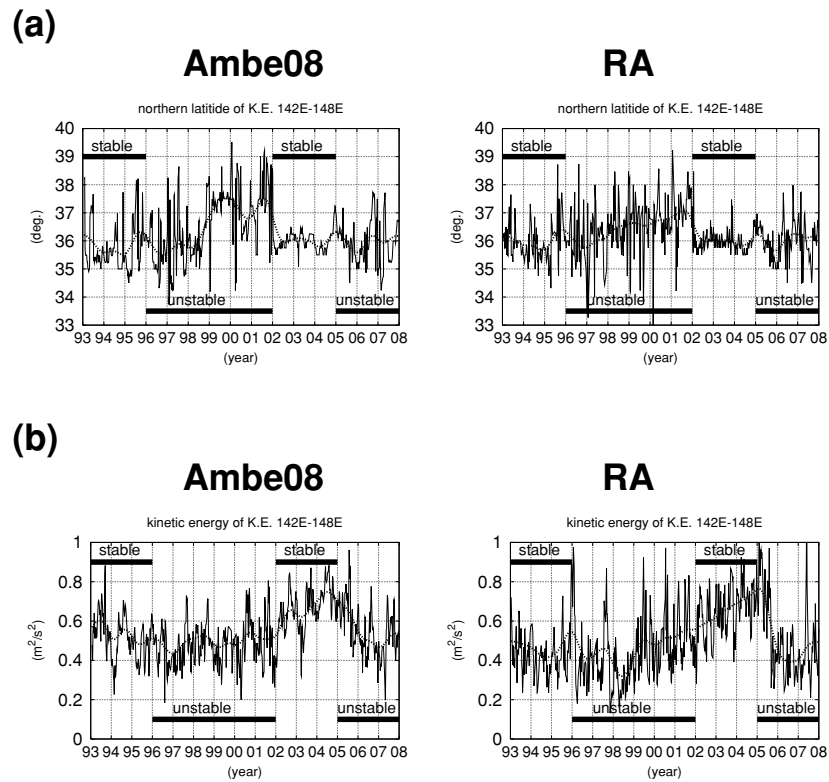


Fig. 9. (a) Time sequence of northernmost latitudes of the first meandering crest of the Kuroshio Extension (FCKE) in 142°–148°E. Left: Ambe08 data. Right: the reanalysis data. (b) As in (a) except for mean kinetic energy along the Kuroshio Extension path between 142° and 148°E. Solid lines denote stable and unstable years of the Kuroshio Extension.

ergy of the first meandering crest of the Kuroshio Extension (hereafter FCKE) in 142°–148°E (Fig. 9). Correlations of the interannual variations of the indices between the reanalysis data and Ambe08 for the northernmost latitude and mean kinetic energy are 0.90 and 0.84, respectively. To quantitatively examine relationships between the dynamical regimes of the Kuroshio Extension and the two indices shown in Fig. 9, we calculated standard deviations for the band-pass-filtered values and temporal averages during the unstable and stable periods (Table 2). Both the reanalysis data and Ambe08 indicate smaller standard deviations for the stable period than for the unstable period. This suggests that the variations on the northernmost latitude and mean kinetic energy of FCKE were stable (unstable) during the stable (unstable) period of the Kuroshio Extension. In addition, during the unstable periods, the mean position of FCKE almost tended to move northward and its mean kinetic energy was lower than when compared with the energy during the stable periods.

4.2 Variability of the Oyashio coastal branch

The Oyashio intrusion along the Japanese east coast

(Oyashio coastal branch; hereafter OY1) varies with seasonal, interannual, and decadal time scales (Yasuda, 2003). We calculated the daily mean sequence of the southern end latitude of the OY1 position (Fig. 10(a)) that is defined as the southern end latitude of grid points with a temperature of 5°C at 100 m depth. The seasonal migration of the southern end latitude of OY1 in the reanalysis data is significant; the climatological monthly mean of reanalysis data (not shown) shows that OY1 reaches to 37.9°N in May and retreats to 41.1°N in December. The monthly mean southern end latitude of OY1 estimated from the observation from 1960 to 2001 moves to 38.8°N in March and April and retreat to 41.2°N in November (Yasuda, 2003). Since the observed southern end latitude of OY1 has the largest interannual variability in April (Yasuda, 2003), we checked the interannual variation of the latitude averaged from March to May. Figure 10(b) compares the averaged southern end latitude with observed data estimated from the in-situ temperature obtained by Japan Meteorological Agency (JMA). Although the reanalysis data showed southward bias of approximately 1° compared with the observation, they reproduced the interannual variation; the correlation

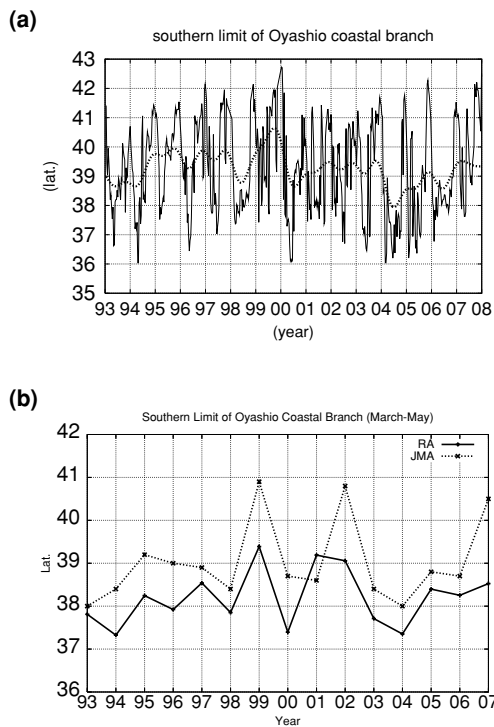


Fig. 10. (a) Time sequences of the southern end latitude of the OY1 estimated from the reanalysis data. The latitude was defined as the southern end latitude of grid points with a temperature of 5°C at 100 m depth in 36°–43°N and 140°–145°E. (b) As in (a) except for mean values from March to May in each year (thick curves with closed squares). Dashed curve with crosses indicates the observation obtained by the Japan Meteorological Agency.

between the reanalysis and observation data is 0.71. Both the reanalysis and observation data indicate that OY1 did not move southward in 1999 as usual but intruded southward in 2004.

We calculated another index: the size of the Oyashio water region (Fig. 11(a)) that is defined as an area of water temperature lower than 5°C at 100 m depth in 36°–43°N and 140°–148°E (JMA, 2006). The size of Oyashio water varies seasonally in a similar manner to the southern end latitude of OY1 and also shows interannual variations. We also compared the size of Oyashio water averaged from March to May for the reanalysis data with the JMA observation data (Fig. 11(b)); the correlation is 0.65. The data well represented two peaks of 1998 and 2006.

4.3 Variability of the North Pacific Intermediate Water (NPIW)

Yasuda *et al.* (1996) indicated that the mixture of low salinity Oyashio water and relatively saline Kuroshio water (old NPIW) along the Kuroshio Extension just off the east coast of Japan can produce new NPIW. The mean

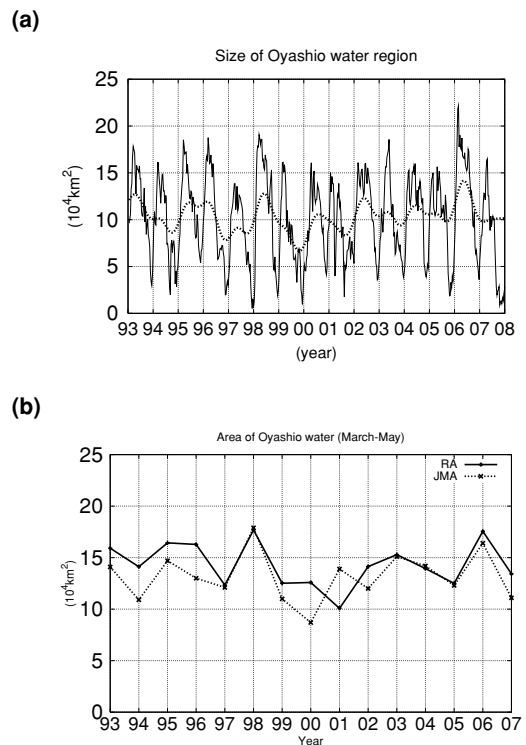


Fig. 11. As in Fig. 10 except for the size of the Oyashio water region that was defined as regions with temperature lower than 5°C at 100 m depth in 36°–43°N and 140°–148°E.

salinity of the reanalysis data at 26.7 σ_θ surface (Fig. 12) shows that the salinity with intermediate value (33.9 < S < 34.1) corresponding to the new NPIW is distributed along the Kuroshio Extension between the lower (S < 33.9) and higher (S > 34.1; old NPIW) salinity waters.

Because spatial variability of salinity at 26.7 σ_θ surface in 36°–43°N and 140°–148°E was large (Fig. 12), we investigated the time sequence of salinity averaged in this region (Fig. 13). The areal mean salinity shows a significant seasonal variation, corresponding well to the seasonal southward intrusion of OY1 (Fig. 10(a)). The interannual variability indicates high (1993–2001 and 2007) and low (2002–2006) salinity periods. The long-term in-situ observation at a section along 41.5°N (JMA, 2006) also showed high (1996–2001) and low salinity periods (2002–2004).

Both FCKE and OY1 highly affect the water mass variability in the mixed water region (Yasuda, 2003). Thus, as shown in Table 3, we checked correlations between the low frequency component of the four indices describing the conditions of FCKE and OY1 (see Subsections 4.1 and 4.2) and that of the mean salinity. The four indices likely have meaningful correlations with the interannual variation of the salinity. Correlations among the four indices (Table 4) indicate that the southern end

latitude of OY1, the eddy kinetic energy in the mixed water region, and the northernmost latitude of FCKE have positive correlations with each other. This is consistent with the dynamics of the mixed water region; the warm core rings sometimes shed from the northward migrating FCKE, and the eddy activity due to the variations of FCKE affects the southward intrusion of OY1. In contrast, the mean kinetic energy of FCKE does not have so meaningful a correlation with the other indices.

To check the statistical relations among the indices in more detail, we calculated the partial correlation coefficients (e.g., Storch and Zwiers, 1999), which describe the regression between two random variables, with the effect of removing a set of controlling random variables. We chose two control variables: the mean kinetic energy of FCKE and the southern end latitude of OY. Both the eddy kinetic energy and the northernmost latitude of FCKE show an increase of positive correlation coefficients controlling the mean kinetic energy of FCKE (third column of Table 3), but show a decrease of positive correlation coefficients controlling the southern end latitude of OY1 (fourth column of Table 3). These results suggest

that the eddy kinetic energy and the northernmost latitude of FCKE were more related to the southern end latitude of OY1 rather than to the mean kinetic energy of FCKE with regard to the effects on the interannual variations of the mean salinity.

To characterize the oceanic conditions of the mixed water region in terms of the interannual variations of the mean salinity at the $26.7\sigma_\theta$ surface, we employed multiple regression analysis. We chose the mean kinetic energy of FCKE and the southern end latitude of OY1 as the explanatory variables according to the estimate of the partial correlation coefficients described above. For 15 values in the middle of June with an interval of 365 days sampled from the low frequency component of the mean salinity, we constructed a regression equation as follows:

$$S_{est} = -0.16E_K + 0.02O_1 + 32.9, \quad (7)$$

where S_{est} , E_K , and O_1 are the mean salinity at the $26.7\sigma_\theta$ surface, mean kinetic energy of FCKE, and southern end latitude of OY1, respectively. The coefficient of multiple determinations in Eq. (7) was 0.80; the t -statistic values

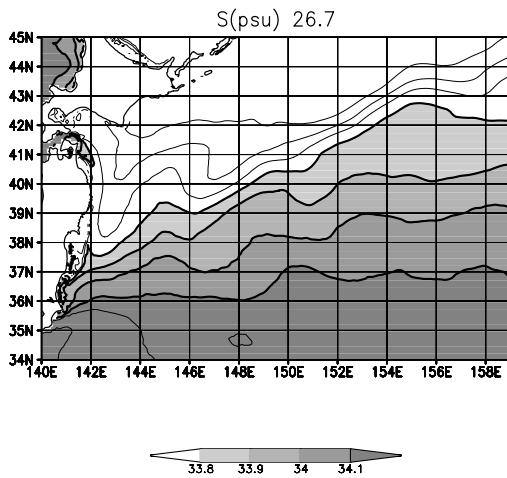


Fig. 12. Mean salinity at $26.7\sigma_\theta$ surface calculated the reanalysis data from 1993 to 2007. Contour interval is 0.1.

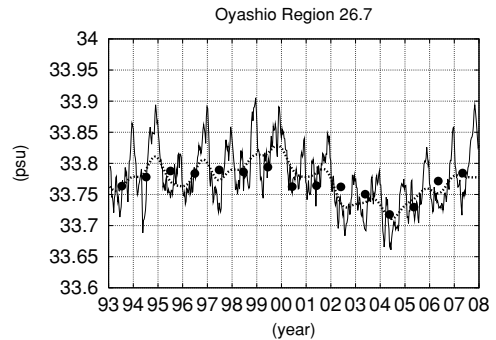


Fig. 13. Time sequences of salinity of the reanalysis data at $26.7\sigma_\theta$ surface averaged over 36° – 43° N and 140° – 148° E. Solid (dashed) curve indicates daily mean values (band-pass-filtered values with periods from 1 year to 10 years). Closed circles indicate the estimation based on the regressive equation (7).

Table 3. Correlation coefficients between the indices associated with the oceanic conditions in the mixed water region and the spatial mean salinity at $26.7\sigma_\theta$ surface. Parentheses in the first column indicate symbols of the indices. Third and fourth columns indicate partial correlation coefficients controlling the southern end latitude of the Oyashio coastal branch (OY1) and mean kinetic energy of the first meandering crest of Kuroshio Extension (FCKE), respectively.

| | Correlation | Partial correlation | Partial correlation |
|---|-------------|---------------------|---------------------|
| Mean kinetic energy of FCKE (MKE) | -0.70 | — | -0.69 |
| Southern end latitude of OY1 (OY1) | 0.64 | 0.62 | — |
| Eddy kinetic energy in the mixed water region (EKE) | 0.56 | 0.70 | 0.42 |
| Northernmost latitude of FCKE (NLFCKE) | 0.45 | 0.61 | 0.34 |

Table 4. Correlation coefficients among four indices: mean kinetic energy of FCKE (MKE), southern end latitude of OY1 (OY1), eddy kinetic energy in the mixed water region (EKE), northernmost latitude of FCKE (NLFCKE).

| | MKE | OY1 | EKE | NLFCKE |
|--------|-------|------|------|--------|
| MKE | — | — | — | — |
| OY1 | -0.31 | — | — | — |
| EKE | -0.09 | 0.42 | — | — |
| NLFCKE | -0.02 | 0.31 | 0.66 | — |

for the coefficients of E_K and O_1 were -3.1 and 2.8 , respectively; the Durbin Watson statistic value of (7) was 1.7 . The salinity values estimated with Eq. (7) were plotted in Fig. 13. The highest (lowest) value of S_{est} in the weak (intense) Oyashio water year 1999 (2004) is characterized by low (high) mean kinetic energy of FCKE and weak (strong) southward intrusion of OY1 (Fig. 14). The new NPIW regions in the weak and intense Oyashio water years are narrow and broad, respectively.

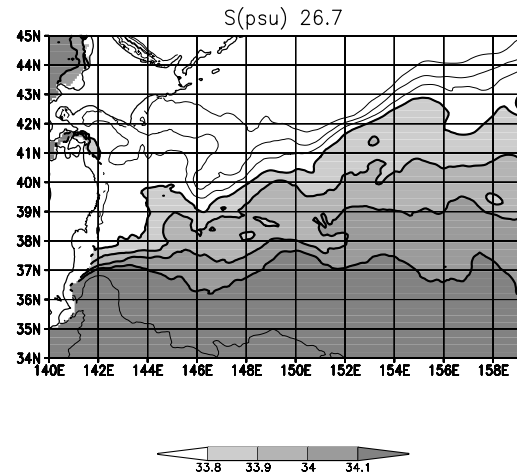
4.4 Variability of the Subtropical Mode Water (SMW)

Although the thickness of SMW in the western North Pacific is basically governed by intensity of the winter monsoon, it is also influenced by the dynamic state of the Kuroshio Extension (Qiu and Chen, 2006; Qiu *et al.*, 2007). In particular, Qiu and Chen (2006) suggested that the dynamic state of the Kuroshio Extension affected the decadal variation of SMW's thickness in the recirculation region of the Kuroshio Extension more strongly than the overlying atmospheric conditions for the period from 1993 to 2004.

The reanalysis data reproduced both the stable and unstable dynamic states of the Kuroshio Extension (Subsection 4.1). With it, we investigated relationships between the interannual variability of SMW and that of the Kuroshio Extension. Figure 15 displays the mean state of the potential vorticity (PV), $(f/\rho_0)(\partial\rho/\partial z)$, (z is the positive value of depth; ρ is the density; ρ_0 is equal to $1025 \text{ kg}\cdot\text{m}^{-3}$; f is the Coriolis parameter) at the $25.4\sigma_\theta$ surface. A closed region south of the Kuroshio Extension with lower PV indicates the SMW region represented in the reanalysis data. Comparison of the reanalysis data with the climatology from in-situ observations (e.g., Suga and Hanawa, 1995a) indicates that the SMW in the reanalysis data shows similar spatial patterns to that observed but its PV value has a positive bias of $1.5\text{--}2.0 \times 10^{-10} \text{ m}^{-1}\text{s}^{-1}$, suggesting that the assimilation process still needs to be improved by adjusting some parameters such as the EOF modes and/or standard deviations of in-situ temperature and salinity included in Eq. (2).

The 15-year variation of PV inside the Kuroshio Extension recirculation gyre in the reanalysis data (Fig.

(a) 1999



(b) 2004

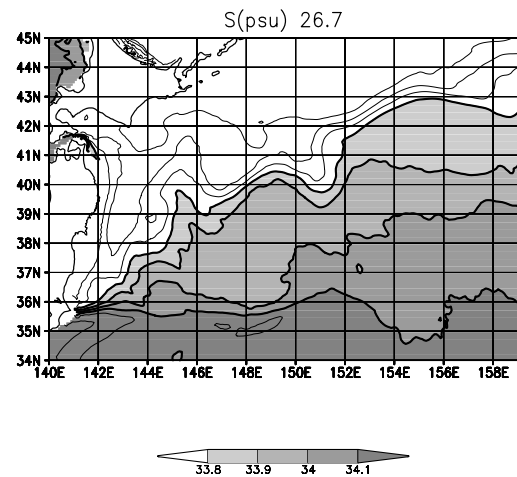


Fig. 14. As in Fig. 12 except for annual mean. (a) in 1999. (b) in 2004.

16) shows that low PV at 300 m depth was intensified in winter during the stable periods (1993 to 1995 and 2002 to 2004) compared with that in the unstable periods (1996 to 2001 and 2005 to 2007). The mixed layer depth in the stable periods tended to be deeper than in the unstable periods. These results are consistent with the analysis using the historical archive of temperature profiles obtained during the period from 1993 to 2005 reported by Qiu and Chen (2006). PV at the $25.4\sigma_\theta$ surface shows the similar interannual variation but it also shows an upward movement of the iso-sigma surface due to heating in the summer season. The correlation coefficients of the time sequence of PV at 300 m depth (Fig. 17) with the northernmost latitude of FCKE (right panel of Fig. 9(a)) and eddy kinetic energy in the mixed water region (Fig. 8)

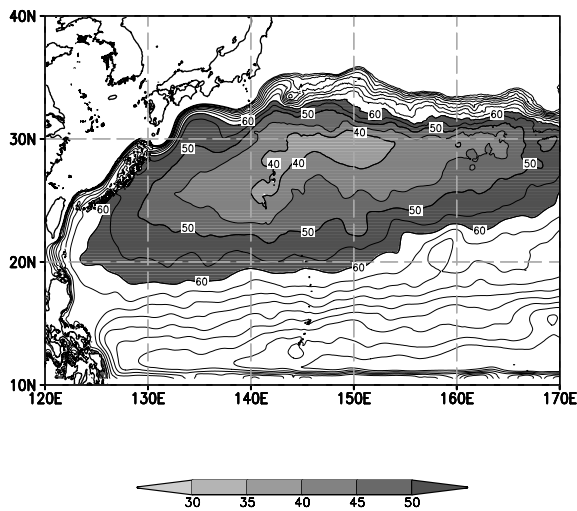


Fig. 15. PV (in $10^{-11} \text{ m}^{-1} \text{ s}^{-1}$) in the reanalysis data at $25.4\sigma_\theta$ surface averaged over the period from 1993 to 2007. The contour interval is $5 \times 10^{-11} \text{ m}^{-1} \text{ s}^{-1}$. A region of PV lower than $60 \times 10^{-11} \text{ m}^{-1} \text{ s}^{-1}$ is shaded.

were 0.77 and 0.61, respectively. This suggests that the reanalysis data well reproduced the relationship between the dynamic state of the Kuroshio Extension and SMW's interannual variability. In contrast, the correlation coefficients with the southern latitude of OY1 (Fig. 10(a)) and mean kinetic energy of FCKE (right panel of Fig. 9(b)) were 0.34 and -0.21 , respectively.

5. Summary and Discussion

By using an eddy-resolving ocean forecast system, JCOPE2, we have created 15-year ocean data of the western North Pacific with a horizontal resolution of $1/12^\circ$ and 46 vertical levels for the period from 1993 to 2007. A combination of a state-of-the-art eddy-resolving ocean general circulation model and the remote and in-situ observation data allowed us to produce realistic high-resolution data (the reanalysis data) of the sea surface height, velocity, temperature, and salinity on the uniform grid over the 15 years period. The reanalysis data well reproduced the mean water mass property included in the in-situ observation in the western North Pacific. It also well reproduced the mean state and interannual variation of the Kuroshio-Kuroshio Extension path and the southern end latitude of OY1.

By analyzing the reanalysis data, we investigated the relationship between the mean salinity in the mixed water region and the behavior of FCKE and of the southern latitude of OY1. Multiple regression analysis suggested that the mean salinity in the mixed water region varied with the interannual time scale responding to both the mean kinetic energy of FCKE and the southern end lati-

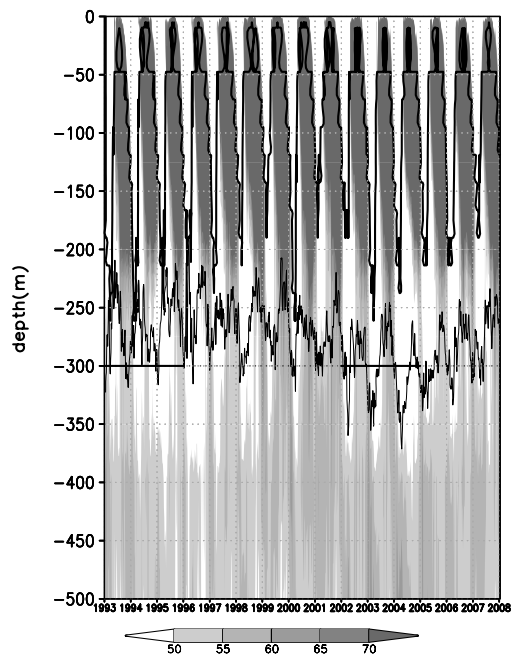


Fig. 16. Time sequence of PV in the reanalysis data inside of the recirculation gyre where SSH subtracted its latitudinal mean was larger than 0.2 m in $30^\circ\text{--}38^\circ\text{N}$ and $140^\circ\text{--}155^\circ\text{E}$. A thick contour denotes the mixed layer depth, defined as the depth at which σ_θ increases by $0.125 \text{ kg}\cdot\text{m}^{-3}$. A thin contour indicates iso-sigma depth of $25.4\sigma_\theta$. Solid (dotted) horizontal lines at 300 m depth denote stable (unstable) periods of the Kuroshio Extension (cf. Fig. 6).

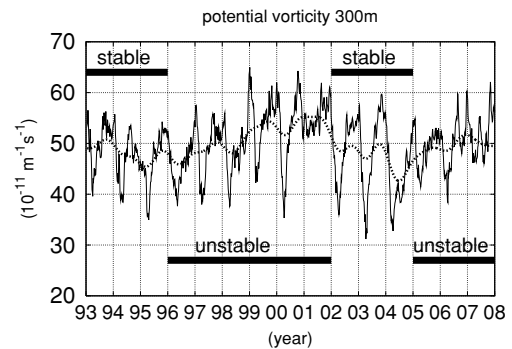


Fig. 17. As in Fig. 8 except for PV at 300 m depth from Fig. 16.

tude of OY1. The horizontal pattern of “new NPIW” in annual mean salinity distribution at $26.7\sigma_\theta$ presented a significant difference between the most saline year of 1999 and the most fresh water year of 2004.

The reanalysis data confirmed the decadal variation of SMW in the Kuroshio Extension recirculation gyre reported by Qiu and Chen (2006). The positive correla-

tion between the interannual migration of the northernmost latitude of FCKE and the PV averaged inside the recirculation gyre at 300 m depth was significant. Because the northernmost latitude of FCKE is closely related with the eddy kinetic energy in the mixed water region, it is suggested that the relationship between the dynamic state of Kuroshio Extension and SMW's thickness in the recirculation region was well reproduced in the reanalysis data.

The regressive equation (7) suggests that not only the southward intrusion of OY1 but also the intensity of FCKE were related to the salinity at $26.7\sigma_\theta$ in the mixed water region. This is consistent with the important roles of the Kuroshio Extension in the formation of the salinity minimum in intermediate layers suggested by previous studies. Using the hydrographic data obtained at repeated observation sections from 1996–2001, Miyao and Ishikawa (2003) indicated that the Oyashio transport of 5.0 Sv mixed with the Kuroshio transport of 10.9 Sv within the layer of $26.6\text{--}27.4\sigma_\theta$ along the Kuroshio Extension at 144°E . Shimizu *et al.* (2004) demonstrated that the Oyashio waters were entrained in the Kuroshio Extension using the data of isopycnal-tracking floats. An OGCM simulation showed the occurrence of isopycnal mixing of the Oyashio and Kuroshio waters along the Kuroshio Extension (Ishizaki and Ishikawa, 2004).

Since it is difficult to use the reanalysis data to investigate the dynamics related to the above relationships, we carried out an additional simulation for the same 15 years but without the data assimilation. The interannual component of intensity of FCKE maintained a meaningful negative correlation (-0.65) with that of the salinity at $26.7\sigma_\theta$ in the 15-year simulation results like that in the reanalysis data. This encourages us to investigate the relevant physical mechanisms included in the simulation results in the near future.

The in-situ data archive used in the present reanalysis (GTSP) did not include most of the data obtained on coastal repeated hydrographic observation lines operationally conducted by prefectural fisheries research agencies (hereafter, FR-DATA). Preliminary assimilation experiments with and without FR-DATA performed by the JCOPE2 system showed that an inclusion of FR-DATA did not affect the large scale features of the oceanic conditions in the mixed water region discussed in the present study but yielded a certain impact on the representation of the local oceanic condition near the Japanese east coast in the mixed water region (Miyazawa *et al.*, 2008b). We also found that very few salinity profiles in the western North Pacific from 1994 to 1999 were archived in the present version of GTSP (Fig. 4). In the near future, we will create another version of the reanalysis data including more additional in-situ data obtained from other sources such as FR-DATA and updated versions of the

World Ocean Database (e.g., Boyer *et al.*, 2006), and further investigate more local water mass variability using it.

Some noticeable biases and RMSEs for in-situ temperature and salinity data were detected in the shelf region of the East China and Okhotsk Seas (Fig. 3). We found that the mixed layer modeling of the JCOPE2 in shallow regions of the marginal seas needed further improvements. Also, the present version of JCOPE2 reanalysis does not assimilate the in-situ data there. The next version of the JCOPE2 reanalysis will use a better mixed layer model and assimilate the in-situ data in the marginal seas.

The JCOPE2 reanalysis data and their updated versions are available from the authors by request. The JCOPE web site (<http://www.jamstec.go.jp/frcgc/jcope/>) provides information about downloading and visualizing the reanalysis data for users.

Acknowledgements

This work is part of the Japan Coastal Ocean Predictability Experiment (JCOPE) promoted by the Japan Agency for Marine-Earth Science and Technology (JAMSTEC). It is also supported by a joint research program (FRA-JCOPE) between the Fisheries Research Agency of Japan (FRA) and JAMSTEC. Dr. T. Kagimoto kindly provided us with FORTRAN codes describing the flux-corrected transport and bi-harmonic schemes for tracer calculations. Dr. K. Uehara also kindly provided us with the bottom topography data of the East China Sea. An anonymous reviewer and the editor Prof. H. Mitsudera provided valuable comments to improve the earlier versions of the manuscript.

Appendix: Adaptive Estimates of the Error Covariance for the Kuroshio-Kuroshio Extension Region

For the Kuroshio-Kuroshio Extension region, we changed the horizontal scales S of the horizontal correlation (3) of the EOF mode adaptively in the assimilation process:

$$S = S^{\min} + (S^{\max} - S^{\min}) \frac{(RMSE_{SSHA}(x, y, t) - RMSE_{SSHA}^{\max})}{(RMSE_{SSHA}^{\min} - RMSE_{SSHA}^{\max})}$$

$$S(x, y, t) = \min(\max(S, S_{\min}), S_{\max}), \quad (\text{A1})$$

where S^{\min} and S^{\max} are the minimum and maximum horizontal scales, respectively; $RMSE_{SSHA}^{\min}$ and $RMSE_{SSHA}^{\max}$ are the critical values of Root Mean Square Error for SSHA observation. Scheme (A1) specifies small horizontal scales at the grid point where RMSE is large. It allowed clear presentation of the sharp fronts of the

Kuroshio, Kuroshio Extension and mesoscale eddies.

In addition, for the Kuroshio-Kuroshio Extension region, we specified the error of SSHA observation adaptively,

$$SSHA_{err}^o = SSHA_{err}^{\min} + \left(SSHA_{err}^{\max} - SSHA_{err}^{\min} \right) \cdot \frac{\left(RMSE_{SSHA}(x, y, t) - RMSE_{SSHA}^{\max} \right)}{\left(RMSE_{SSHA}^{\min} - RMSE_{SSHA}^{\max} \right)}$$

$$SSHA_{err}^o(x, y, t) = \min\left(\max\left(SSHA_{err}^o, SSHA_{err}^{\min}\right), SSHA_{err}^{\max}\right), \quad (A2)$$

where $SSHA_{err}^{\min}$ and $SSHA_{err}^{\max}$ are the lower and upper limits of the observation error, respectively. Scheme (A2) was also useful for the sharp presentation of the oceanic fronts.

References

- Ambe, D., S. Imawaki, H. Uchida and K. Ichikawa (2004): Estimating the Kuroshio axis south of Japan using combination of satellite altimetry and drifting buoys. *J. Oceanogr.*, **60**, 375–382.
- Bloom, S. C., L. L. Takacs, A. M. da Silva and D. Ledvina (1996): Data assimilation using Increment Analysis Updates. *Mon. Wea. Rev.*, **124**, 1256–1271.
- Boris, J. P. and D. L. Book (1973): Flux-corrected transport I: SHASTA, a fluid transport algorithm that works. *J. Comput. Phys.*, **11**, 38–69.
- Boyer, T. P., J. I. Antonov, H. E. Garcia, D. R. Johnson, R. A. Locarnini, A. V. Mishonov, M. T. Pitcher, O. K. Baranova and I. V. Smolyar (2006): World Ocean Database 2005. NOAA Atlas NESDIS 60, ed. by S. Levitus, U.S. Government Printing Office, Washington, D.C., 190 pp., DVDs.
- Carton, J. A. and A. Santorelli (2008): Global decadal upper-ocean heat content as viewed in nine analyses. *J. Climate*, **21**, 6015–6035.
- Conkright, M. E., J. I. Antonov, O. Baranova, T. P. Boyer, H. E. Garcia, R. Gelfeld, D. Johnson, R. A. Locarnini, P. P. Murphy, T. D. O'Brien, I. Smolyar and C. Stephens (2002): World Ocean Database 2001, Volume 1: Introduction. NOAA Atlas NESDIS 42, ed. by S. Levitus, U.S. Government Printing Office, Washington, D.C., 167 pp.
- Daley, R. (1991): *Atmospheric Data Analysis*. Cambridge University Press, New York, 472 pp.
- Ebuchi, N., Y. Fukamachi, K. Ohshima, K. Shirasawa, M. Ishikawa, T. Takatsuka, T. Daibo and M. Wakatsuchi (2006): Observation of the Soya Warm Current using HF Ocean Radar. *J. Oceanogr.*, **62**, 47–61.
- Ezer, T. and G. L. Mellor (1994): Continuous assimilation of Geosat altimeter data into a three-dimensional primitive equation Gulf Stream model. *J. Phys. Oceanogr.*, **24**, 832–847.
- Feder, T. (2000): Argo begins systematic global probing of the upper oceans. *Phys. Today*, **53**, DOI:10.1063/1.1292477.
- Fujii, Y. and M. Kamachi (2003): A reconstruction of observed profiles in the sea east of Japan using vertical coupled temperature-salinity EOF modes. *J. Oceanogr.*, **59**, 173–186.
- Griffies, S. M. and R. W. Hallberg (2000): Biharmonic friction with a Smagorinsky-like viscosity for use in large-scale eddy-permitting ocean models. *Mon. Wea. Rev.*, **128**, 2935–2946.
- Guo, X., H. Hukuda, Y. Miyazawa and T. Yamagata (2003): A triply nested ocean model simulating the Kuroshio—Roles of horizontal resolution on JEBAR—. *J. Phys. Oceanogr.*, **33**, 146–169.
- Hasunuma, K. (1978): Formation of the intermediate salinity minimum in the northwestern Pacific Ocean. *Bull. Ocean Res. Inst., Univ. of Tokyo*, **9**, 47 pp.
- Hinada, T. (1996): Seasonal variation and long-term trends of the oceanographic conditions along a fixed hydrographic line crossing the Kuroshio in the East China Sea. *Oceanogr. Mag.*, **45**, 9–32.
- Ichikawa, H., H. Nakamura, A. Nishina and M. Higashi (2004): Variability of northeastward current southeast of northern Ryukyu Islands. *J. Oceanogr.*, **60**, 351–363.
- Imawaki, S., H. Uchida, H. Ichikawa, M. Fukasawa, S. Umatani and ASUKA Group (2001): Satellite altimeter monitoring the Kuroshio transport south of Japan. *Geophys. Res. Lett.*, **28**(1), 17–20.
- Ishizaki, H. and I. Ishikawa (2004): Simulation of formation and spreading of salinity minimum associated with NPIW using a high-resolution model. *J. Oceanogr.*, **60**, 463–485.
- Japan Meteorological Agency (2006): '2.2.3 Oyashio'. In *Japan Meteorological Agency Comprehensive Oceanographic Information* (in Japanese). http://www.data.kishou.go.jp/kaiyou/shindan/sougou/pdf/S22_2.2.3.pdf
- Kagimoto, T., Y. Miyazawa, X. Guo and H. Kawajiri (2008): High resolution Kuroshio forecast system—Description and its applications—. p. 209–234. In *High Resolution Numerical Modeling of the Atmosphere and Ocean*, ed. by W. Ohfuchi and K. Hamilton, Springer, New York.
- Kalnay, E. and Coauthors (1996): The NCEP/NCAR 40-year reanalysis project. *Bull. Amer. Meteor. Soc.*, **77**, 437–471.
- Kuragano, T. and M. Kamachi (1999): Global statistical space-time scales of oceanic variability estimated from the TOPEX/POSEIDON altimetry data. *J. Geophys. Res.*, **105**, 955–974.
- Masuzawa, J. (1969): Subtropical Mode Water. *Deep-Sea Res.*, **16**, 463–472.
- McCalpin, J. D. (1994): A comparison of second-order and fourth-order pressure gradient algorithms in a sigma coordinate ocean model. *Int. J. Num. Methods Fluids*, **18**, 361–383.
- Mellor, G., T. Ezer and L.-Y. Oey (1994): The pressure gradient conundrum of sigma coordinate ocean models. *J. Atmos. Oceanic Technol.*, **11**, 1126–1134.
- Mellor, G. L., S. Hakkinen, T. Ezer and R. Patchen (2002): A generalization of a sigma coordinate ocean model and an intercomparison of model vertical grids. p. 55–72. In *Ocean Forecasting: Conceptual Basis and Applications*, ed. by N. Pinardi and J. D. Woods, Springer, New York.
- Mitsudera, H., B. Taguchi, Y. Yoshikawa, H. Nakamura, T. Waseda and T. Qu (2004): Numerical study on the Oyashio

- water pathways in the Kuroshio-Oyashio Confluence. *J. Phys. Oceanogr.*, **34**, 1174–1196.
- Miyao, T. and K. Ishikawa (2003): Formation, distribution and volume transport of the North Pacific Intermediate Water studied by repeat hydrographic observations. *J. Oceanogr.*, **59**, 905–919.
- Miyazawa, Y. (2007): Development of numerical ocean forecasting technique—Kuroshio, Oyashio, and the Indian Ocean—. *Suiro (Hydrology)*, **142**, 22–34 (in Japanese).
- Miyazawa, Y., X. Guo and T. Yamagata (2004): Roles of mesoscale eddies in the Kuroshio paths. *J. Phys. Oceanogr.*, **34**, 2203–2222.
- Miyazawa, Y., S. Yamane, X. Guo and T. Yamagata (2005): Ensemble forecast of the Kuroshio meandering. *J. Geophys. Res.*, **110**, C10026, doi:10.1029/2004JC002426.
- Miyazawa, Y., T. Kagimoto, X. Guo and H. Sakuma (2008a): The Kuroshio large meander formation in 2004 analyzed by an eddy-resolving ocean forecast system. *J. Geophys. Res.*, **113**, C10015, doi:10.1029/2007JC004226.
- Miyazawa, Y., K. Komatsu and T. Setou (2008b): Nowcast skill of the JCOPE2 ocean forecast system in the Kuroshio-Oyashio mixed water region. *J. Marine Meteorol. Society (Umi to Sora)*, **84**, 85–91 (in Japanese with English abstract and figure captions).
- Mizuno, K. and W. B. White (1983): Annual and interannual variability in the Kuroshio Current system. *J. Phys. Oceanogr.*, **13**, 1847–1867.
- Nakano, T., I. Kaneko, M. Endoh and M. Kamachi (2005): Interannual and decadal variabilities of NPIW salinity minimum core observed along JMA's hydrographic repeat sections. *J. Oceanogr.*, **61**, 681–697.
- Oey, L.-Y. and P. Chen (1992): A nested-grid ocean model: with application to the simulation of meanders and eddies in the Norwegian Coastal Current. *J. Geophys. Res.*, **97**, 20,063–20,086.
- Qiu, B. and S. Chen (2006): Decadal variability in the formation of the North Pacific Subtropical Mode Water: Oceanic versus atmospheric control. *J. Phys. Oceanogr.*, **36**, 1365–1380.
- Qiu, B., S. Chen and P. Hacker (2007): Effect of mesoscale eddies on Subtropical Mode Water variability from the Kuroshio Extension System Study (KESS). *J. Phys. Oceanogr.*, **37**, 982–1000.
- Reid, J. L., Jr. (1965): Intermediate waters of the Pacific Ocean. *The Johns Hopkins Oceanographic Studies*, **5**, 96 pp.
- Shikama, N. (1994): Current measurement in the Tsugaru Strait using bottom-mounted ADCPs. *Kaiyo Monthly*, **26**, 815–818 (in Japanese).
- Shimizu, Y., T. Iwao, I. Yasuda, S. Ito, T. Watanabe, K. Uehara, N. Shikama and T. Nakano (2004): Formation process of North Pacific Intermediate Water revealed by profiling floats set to drift on $26.7\sigma_\theta$ isopycnal surface. *J. Oceanogr.*, **60**, 453–462.
- Storch, H. and F. Zwiers (1999): *Statistical Analysis in Climate Research*. Cambridge University Press, Cambridge, 484 pp.
- Suga, T. and K. Hanawa (1995a): The subtropical mode water circulation in the North Pacific. *J. Phys. Oceanogr.*, **25**, 958–970.
- Suga, T. and K. Hanawa (1995b): Interannual variations of North Pacific Subtropical Mode Water in the 137°E section. *J. Phys. Oceanogr.*, **25**, 1012–1017.
- Takikawa, T., J. H. Yoon and K. D. Cho (2005): The Tsushima warm current through Tsushima straits estimated from ferryboat ADCP data. *J. Phys. Oceanogr.*, **35**, 1154–1168.
- Talley, L. D. (1993): Distribution and formation of North Pacific Intermediate Water. *J. Phys. Oceanogr.*, **23**, 517–537.
- Tatebe, H. and I. Yasuda (2004): Oyashio southward intrusion and cross-gyre transport related to diapycnal upwelling in the Okhotsk Sea. *J. Phys. Oceanogr.*, **34**, 2327–2341.
- Uchida, H. and S. Imawaki (2003): Eulerian mean surface velocity field derived by combing drifter and satellite altimeter data. *Geophys. Res. Lett.*, **30**, 1229, doi:10.1029/2002GL016445.
- Uda, M. (1963): Oceanography of the subarctic Pacific region. *J. Fish. Res. Board Can.*, **20**, 119–179.
- Uehara, K., Y. Saito and K. Hori (2002): Paleotidal regime in the Changjiang (Yangtze) Estuary, the East China Sea, and the Yellow Sea at 6 ka and 10 ka estimated from a numerical model. *Mar. Geol.*, **183**, 179–192.
- Uehara, K., S. Ito, H. Miyake, I. Yasuda, Y. Shimizu and T. Watanabe (2004): Absolute volume transports of the Oyashio referred to moored current meter data crossing the OICE. *J. Oceanogr.*, **60**, 397–409.
- Usui, N., S. Ishizaki, Y. Fujii, H. Tsujino, T. Yasuda and M. Kamachi (2006): Meteorological Research Institute multivariate ocean variational estimation (MOVE) system: Some early results. *Adv. Space Res.*, **37**, 806–822, doi:10.1016/j.asr.2005.09.022.
- Wang, Y. H., S. Jan and D. P. Wang (2003): Transports and tidal current estimates in the Taiwan Strait from shipboard ADCP observations (1999–2001). *Estuar., Coast. Shelf Sci.*, **57**, 193–199.
- Yasuda, I. (1997): The origin of the North Pacific Intermediate Water. *J. Geophys. Res.*, **102**, 893–909.
- Yasuda, I. (2003): Hydrographic structure and variability in the Kuroshio-Oyashio transition area. *J. Oceanogr.*, **59**, 389–402.
- Yasuda, I., K. Okuda and Y. Shimizu (1996): Distribution and modification of the North Pacific Intermediate Water in the Kuroshio-Oyashio Interfrontal zone. *J. Phys. Oceanogr.*, **26**, 448–465.
- Yoshida, K. (1964): A note on the variations of the Kuroshio during recent years. *Bull. Jpn. Soc. Fish Oceanogr.*, **5**, 66–69 (in Japanese).
- Yoshinari, H., I. Yasuda and M. Ikeda (2004): Meridional transport of North Pacific Intermediate Water across 37°N based on an objective analysis of lowered acoustic Doppler current profiler data. *J. Geophys. Res.*, **109**, C02023, doi:10.1029/2003JC001815.
- Yoshinari, H., T. Setou, A. Okuno, D. Ambe, K. Komatsu, Y. Miyazawa and FRA-JCOPE group (2008): Impact evaluation of Argo data for reproducibility of FRA-JCOPE. *J. Marine Meteorol. Society (Umi to Sora)*, **84**, 77–84 (in Japanese with English abstract and figure captions).
- Zhu, X.-H., I.-S. Han, J.-H. Park, H. Ichikawa, K. Murakami, A. Kaneko and A. Ostrovskii (2003): The northeastward current southeast of Okinawa Island observed during November 2000 to August 2001. *Geophys. Res. Lett.*, **30**(23), 1071, doi:10.1029/2002GL015867.